

Article

Development History of the Loess–Paleosol Profiles of Pécel, Kisdorog and Bonyhádvarasd, Hungary

László Makó ^{1,2,*}, Péter Cseh ^{1,2}, Balázs Nagy ^{1,2}, Pál Sümegei ^{1,2} and Dávid Molnár ^{1,2,*} 

- ¹ Department of Geology and Paleontology, University of Szeged, Egyetem u. 2-6, H-6722 Szeged, Hungary; cspeti94@gmail.com (P.C.); nagba88@gmail.com (B.N.); sumegi@geo.u-szeged.hu (P.S.)
- ² Interdisciplinary Centre of Excellence, Institute of Geography and Earth Sciences, Long-Term Environmental Changes Research Group, University of Szeged, Egyetem u. 2-6, H-6722 Szeged, Hungary
- * Correspondence: makol@geo.u-szeged.hu (L.M.); molnard@geo.u-szeged.hu (D.M.)

Abstract: This study covers the examination of four loess–paleosol profiles in Hungary through grain size composition, organic matter, carbonate content and magnetic susceptibility measurements. One of the profiles (with a thickness of 25.72 m) can be found in the Gödöllő hills, on the border of town Pécel, and the other three profiles (Kisdorog–West—5.60 m, Kisdorog–East—6.40 and Bonyhádvarasd—8.16 m) are located in the Tolna hills of the Transdanubia region. The sections were continuously sampled with an interval of 4 cm. The same interval was also applied to the other three profiles. During the field exploration of the Pécel profile, we were able to study the complete loess wall, which was deposited on the sediment of the nearby Rákos stream. Based on the Ostracod fauna of the clay sediment beneath, the fluvial deposit can be considered as originating from the Upper Miocene. In the case of the Transdanubian sections, a significant change can be observed in the prevailing wind direction based on the grain size analyses. In addition, the results of magnetic susceptibility measurements suggest that the development of the Pécel profile took place during MIS 9–10, while the age of the three Transdanubian sections can be assumed to be the MIS 2–4.

Keywords: loess–paleosol; Pécel; Kisdorog; Bonyhádvarasd; grain size



Citation: Makó, L.; Cseh, P.; Nagy, B.; Sümegei, P.; Molnár, D. Development History of the Loess–Paleosol Profiles of Pécel, Kisdorog and Bonyhádvarasd, Hungary. *Quaternary* **2023**, *6*, 38. <https://doi.org/10.3390/quat6030038>

Academic Editor: James B. Innes

Received: 30 May 2023

Revised: 22 June 2023

Accepted: 27 June 2023

Published: 2 July 2023



Copyright: © 2023 by the authors. Licensee MDPI, Basel, Switzerland. This article is an open access article distributed under the terms and conditions of the Creative Commons Attribution (CC BY) license (<https://creativecommons.org/licenses/by/4.0/>).

1. Introduction

The four profiles examined in this study can be found in two different geographical regions of Hungary (Figure 1). One of them can be found in the vicinity of the town Pécel in the Gödöllő hills area [1] in a foothill location (e.g., [2–6]), while the other three profiles are located in the Tolna hills [7] in a lowland location (e.g., [8–15]). In addition to the one in Pécel, two of the examined sections are located in Kisdorog and one in Bonyhádvarasd, 130–140 km away from Pécel. In the case of these Transdanubian sections, the direction of the hills in the area is northwest–southeast.

Detailed pieces of information on the loess sequences of the Carpathian Basin are available (e.g., [2,3,6,8–10,14–21]), however, the sections we examined have not been studied before, thus, the data extracted from them could provide excellent additional information about the paleoclimate and regional mosaicism of the area. Several profiles have been studied along the River Danube [2,14,15,18], the data of which were supplemented by data from southern Hungary [6,8–10,12,13], northern Hungary [3–5,22], Transdanubia [6,11,14,15], and data derived from drillings [23,24].

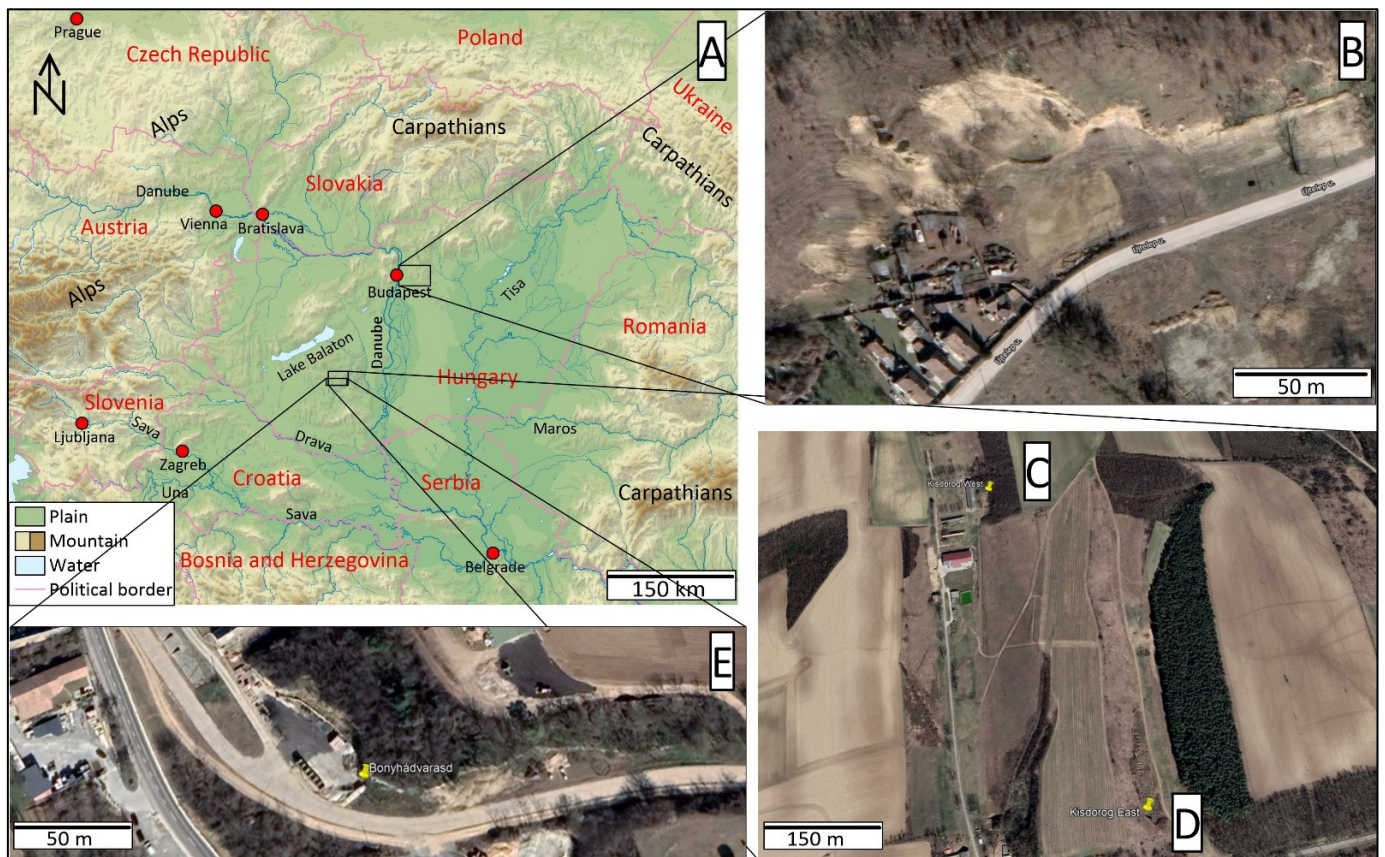


Figure 1. Location of the loess–paleosol section of Pécel ((B)—orthophotomap), Kisdorog-West ((C)—orthophotomap), Kisdorog-East ((D)—orthophotomap) and Bonyhádvarasd ((E)—orthophotomap) in the Carpathian Basin (A) [25].

The excavation of the loess–paleosol profile of Pécel was completed in 2022. Prior to this, its preliminary results were reported in 2021 [22]. The total height of this section is 25.72 m, of which the actual loess deposit was 24.56 m. The sediments (thickness: 51 cm) below this loess section can be considered as the sediments of the former Rákos stream, which recently can be found 300–350 m south of the loess wall. This further deepening of the profile was considered irrelevant since the main purpose of this research is the reconstruction of the development of the loess wall itself. Regardless, the development of the former riverbed below the loess wall could also be clearly reconstructed by the analysis of its sediments. The bottom 65 cm of it consists of clay, while sand with massive, cross-layered and laminated features can be described in the upper 51 cm. Based on the experiences of previous research on loess bodies and similar sediment depositions, the higher resolution of sampling enables a higher resolution of examination (e.g., [8–12]). We have therefore sought to achieve the highest possible resolution—of course within reasonable limits. Thus, a sampling interval of 4 cm was applied, which can result in the resolution of decades-to-centuries if it is supplemented with well-designed radiocarbon age data (e.g., [4,8–12,26]). The loess–paleosol profiles near Kisdorog (Figure 1) are located in the midwest region of Hungary at $46^{\circ}23'54''$ N and $18^{\circ}29'47''$ E (Kisdorog-West) and $46^{\circ}23'34''$ N and $18^{\circ}30'01''$ E (Kisdorog-East). The two profiles can be found on the opposite slopes of a hill, approximately 700 m from each other. The Kisdorog-West section can be characterized by a height of 5.6 m. One single paleosol layer of about 1 m thickness can be found in it, which can be divided further into 3 sublayers. The Kisdorog-East section can be characterized by a height of 6.4 m, within which a single paleosol layer can be separated similar to the western section. This paleosol layer of 3 m can also be separated into 3 sublayers. The fourth section can be found in Bonyhádvarasd, which is located

3.5 km away from Kisdorog. The coordinates of the Bonyhádvarasd section of 8.16 m height are 46°21'52" N and 18°29'17" E. Similar to the Kisdorog sections, it can also be divided into lower and upper loess bodies separated by a paleosol complex.

2. Materials and Methods

The Pécel section (Figure 1) (47°29'47" N and 19°21'12" E) was supplemented by a 10th subsection (with a height of 700 cm). This section was also sampled for grain size distribution and LOI analysis by applying the previously used 4 cm sample size.

2.1. Color

During the field studies, following the cleaning of the entire wall surface, the visible layers and their boundaries were registered and their colors were defined according to the Munsell color chart [27]. These macroscopic observations were the basis of the delimitation of the different layers. In the case of the Pécel profile, the paleosols [28–30] ranged from brown to reddish-brown, while in the case of the Kisdorog and Bonyhádvarasd profiles, the paleosols showed three different colors, ranging from chestnut brown to dark brown, indicating significant soil development. In addition, the color of the loess also differed (whitish–pale yellow) in the case of the Bonyhádvarasd profile. Our research was primarily focused on the study of the loess material, thus, detailed pedological examination of the paleosol layers has not been carried out.

2.2. LOI

Dean's Loss on Ignition method [31] was used to determine the organic matter and carbonate content of the samples. This method is based on the measurement of the loss on ignition weight of the powdered sediment samples. The previously air-dried samples are first ignited at 550 °C, at which temperature the organic matter is being burnt, and then, at 900 °C, in order to detect the carbonate content. The 900 °C temperature value was chosen based on the study of Heiri et al. [32]. Regardless, the heating of the samples was performed at both 900 and 1000 °C, resulting in two different series of measurements. The average weight loss was plus 0.0007 g at 1000 °C. This difference can be explained by water present in clay minerals, as well as in crystalline bonds, in which water content is likely to escape from the system at this applied temperature. These measurements were carried out by using a furnace at the Department of Geology and Paleontology of the University of Szeged.

2.3. Grain Size Distribution

For the analysis of the grain size composition, the samples were prepared according to the method of Bokhorst et al. [33]. Air-dry samples were pre-treated in a 30% H₂O₂ and then a 10% HCl bath to remove organic matter and carbonates before further analysis. Subsequently, 30 mL of 5% Calgon (Na₂P₆O₁₈) was added to 0.7 g of the sample in order to separate the particles. Right before the measurements, the samples were treated in an ultrasonic cleaner for 10 min to prevent the coagulation of the particles. The grain size composition measurements were carried out by using an OMEC EasySizer 20 laser sedimentograph at the Department of Geology and Paleontology, University of Szeged. The source was a He-Ne laser with an energy of 2 MW and a wavelength of 0.6328 μm. The Laser Sedigraph uses 54 built-in detectors for measuring a range of 42 grain size fractions between 0.0001 and 0.5 mm. The approach is based on the theory of Mie laser light scattering. Following the measurements, the system calculates cumulative values by using the measurement results. The values obtained were organized into grain size fractions according to the Wentworth scale [34].

2.4. Grain Size Indices

The average particle size (MGS) was calculated from the values of D₁₀-D₅₀-D₇₅ and plotted with a line diagram. The U-ratios and the GSI values were calculated by

using the grain size composition results in order to determine the energy of the transport medium [35–37].

The U-ratio defines the ratio of the coarse silt and the medium + fine silt fractions. This ratio can be applied to distinguish the cold, dry glacial periods with significant eolian transport and high wind velocity (high U-ratio), and the warm, wet interglacial periods with weak wind intensity (low U-ratio). This distinction approach is based on the observation that the predominant grain size fraction of eolic sedimentation is $<16\ \mu\text{m}$ in warmer interglacial periods, while it is $>16\ \mu\text{m}$ in colder glacial periods [36,38]. Clay fraction ($<5.5\ \mu\text{m}$) and grain size fractions coarser than $44\ \mu\text{m}$ are not taken into account for the calculation of the U-ratio, thus, no information can be obtained about clay minerals formed by secondary pedogenetic processes or about fine sand particles transported in saltation [36,39].

The Grain Size Index (GSI) introduced by Rousseau et al. [40] is similar to the U-ratio. The most significant difference is that the clay fraction is also taken into account for its calculation. Based on this index, the efficiency of sedimentation, transport and accumulation processes can be determined which are closely related to the changes in wind velocity [41]. High GSI values indicate an increased frequency and intensity of dust storms, as well as a higher sedimentation rate [41,42].

2.5. Magnetic Susceptibility

The magnetic susceptibility [43–50] measurements were carried out by using a Bartington MS2K surface sensor instrument at the Department of Geology and Paleontology, University of Szeged. The air-dried, powdered samples were measured three times in different directions.

3. Results

3.1. Profiles

3.1.1. Pécel

The notations of Chinese loess sections [18,51–53] were used for the description of the lithological horizons. The lowest 65 cm of the section (between 25.07–25.72 m) is clay sediment, which is followed by 51 cm of sand sediment above it (between 24.56 and 25.07 m). Above this, the development of loess (between 0 and 24.56 m) starts with a hiatus in some places. The lowest stratum denoted as L6, is located between 23.48 and 24.56 m and is characterized by a Munsell color of 7.5YR 7/4. Above it, 28 cm of paleosol (S5, between 23.20 and 23.48 m) can be found with 10YR 5/6 color. The loess body L5 is located between 19.36 and 23.20 m and its color is 7.5YR 7/3. The S4 paleosol between 19.08 and 19.36 m has a 10YR 5/6 color, similar to the S5. The L4 stratum between 18.72 and 19.08 m is a 7.5YR 7/3 colored loess again. Above the L4 loess body, the S3 paleosol layer can be found, which consists of two parts, the lower one (between 18.44 and 18.72 m) with 2.5Y 6/4 color, the upper one (between 17.84 and 18.44 m) with 2.5Y 5/3 color. The loess body above this (L3) can be found between 15.40 and 17.84 m and can be characterized by 2.5Y 7/4 color. The S2 paleosol also consists of two parts, the lower one (between 14.52 and 15.40 m) with 10YR 6/4 color, and the upper one (between 14.16 and 14.52 m) with 10YR 5/2 color. The loess body L2 is located between 12.56 and 14.16 m and has a color of 2.5Y 7/3. The S1 paleosol can be divided into 6 different parts based on its color: 10YR 6/6 (11.80–12.6 m); 10YR 5/6 (11.24–11.80 m); 10YR 6/6 (10.44–11.24 m); 10YR 5/6 (10.00–10.41 m); 2.5Y 6/4 (9.32–10.00 m) and 2.5Y 5/3 (8.84–9.32 m) The overlying sedimentary layer was described as a well-observable loess body with a layer of paleosol in it. L1L2, which can be characterized by 2.5Y 7/4 color, is located between 5.64 and 8.84 m. The paleosol layer in-between denoted as L1S1 (color: 10YR 6/6) can be found between 3.00 and 5.64 m. Above it, the uppermost loess layer (L1L1) between 0.44 and 3.00 m can be characterized with 2.5Y 7/4 color again. The uppermost stratum of the entire sequence is the recent soil layer with a thickness of 44 cm which can be described with 2.5Y 6/4 color between 0.20 and 0.44, and 2.5Y 5/3 between the surface and 0.20 m.

3.1.2. Kisdorog-West

This profile is between 3.84 and 5.6 m of a loess wall of 5.6 m total height, with large carbonate concretions I from the depth of 5.5 m. A notable paleosol horizon can be found between 2.32 and 3.84 m. The lower part (between 3.28 and 3.84 m) of this paleosol can be characterized by chestnut brown color (7.5YR 3/6), while the middle part of it (2.52–3.28 m) is dark brown (2.5Y 2/2). Several carbonate concretions can be found in these two lower layers between 3 and 3.9 m. The uppermost part of the paleosol layer between 2.32 and 2.52 can be characterized by light brown color (2.5Y 3/2). The upper loess body of the profile (0.4–2.32 m) can be found above the paleosol layer. Above, the uppermost 0.4 m is the recent soil horizon. In these two uppermost layers, several rhizoliths can be observed between 0 and 1.3 m.

3.1.3. Kisdorog-East

The lowermost 0.20 m of this profile with a height of 6.4 m is a loess layer (between 6.2 and 6.4 m). A notable paleosol horizon can be found between 2.72 and 6.2 m, which can be divided further into sublayers. The following sublayers can be distinguished based on their colors: chestnut brown (7.5YR 3/6) between 5.84 and 6.2 m, dark brown (2.5Y 2/2) between 4.6 and 5.84 m, light brown (2.5Y 3/2) between 4.2 and 4.6 m, and dark brown again between 3.16 and 4.2 m with crotonines between 3.24 and 3.3 m. The uppermost paleosol layer can be found between 2.72 and 3.16 m and can be characterized by light brown color. The upper loess layer can be found between 0.36 and 2.72 m, which is followed by the recent surface soil (0 and 0.36 m).

3.1.4. Bonyhádvarasd

This profile of 8.16 m total height can be described with the presence of a loess layer in the lower position (6.08–8.16 m) and a paleosol layer between 3.76 and 6.08 m, which latter can also be divided into further sublayers. These certain sublayers were defined by their colors, which are the followings: chestnut brown (7.5YR 3/6, between 5.52 and 6.08 m), dark brown (2.5Y 2/2, between 5.2 and 5.4 m), light brown with lime spots (2.5Y 3/2, between 4.84 and 4.96 m), dark brown (2.5Y 2/2, between 3.76 and 4.36 m) and chestnut brown with rhizoliths (7.5YR 3/6, between 3.76 and 4.36 m). The upper loess layer can be found above the paleosol horizon (between 0.15 and 3.76 m) with carbonate concretions in its lower parts. The uppermost 0.15 m of the section can be described as another paleosol horizon.

3.2. LOI

3.2.1. Pécel

The upper 18.72 m of the loess–paleosol profile of Pécel was previously studied and published [22], thus, only the newly obtained results are presented in this paper (Figure 2).

Greyish-brown clay sediment can be found in the range 25.07–25.72 m where the organic matter content varies in the range 1.2–2.7%. The carbonate content gradually increases towards the sand layer deposited on the top of the clay (~7 to 11% to 2.5%).

The lowest organic matter (0.4–1%) and carbonate (0.7–2.5%) content values can be detected in this sand body in the range 24.56–25.07 m. Subsequently, the lowermost loess body (L6) is located in the range 23.48–24.56 m, in which organic matter (1–2%) and carbonate (1.7–5%) show relatively constant values. Both organic matter and carbonate content values constantly increase up to the level of the next paleosol horizon above this loess layer.

A thinner paleosol layer (S5) can be found in the range 23.20–23.48 m, in which the organic matter varies in the range 2.3–2.7%, while the carbonate content shows a more significant increase and rises from 5.8 to ~8%. The increased values of the latter persist in the overlying loess.

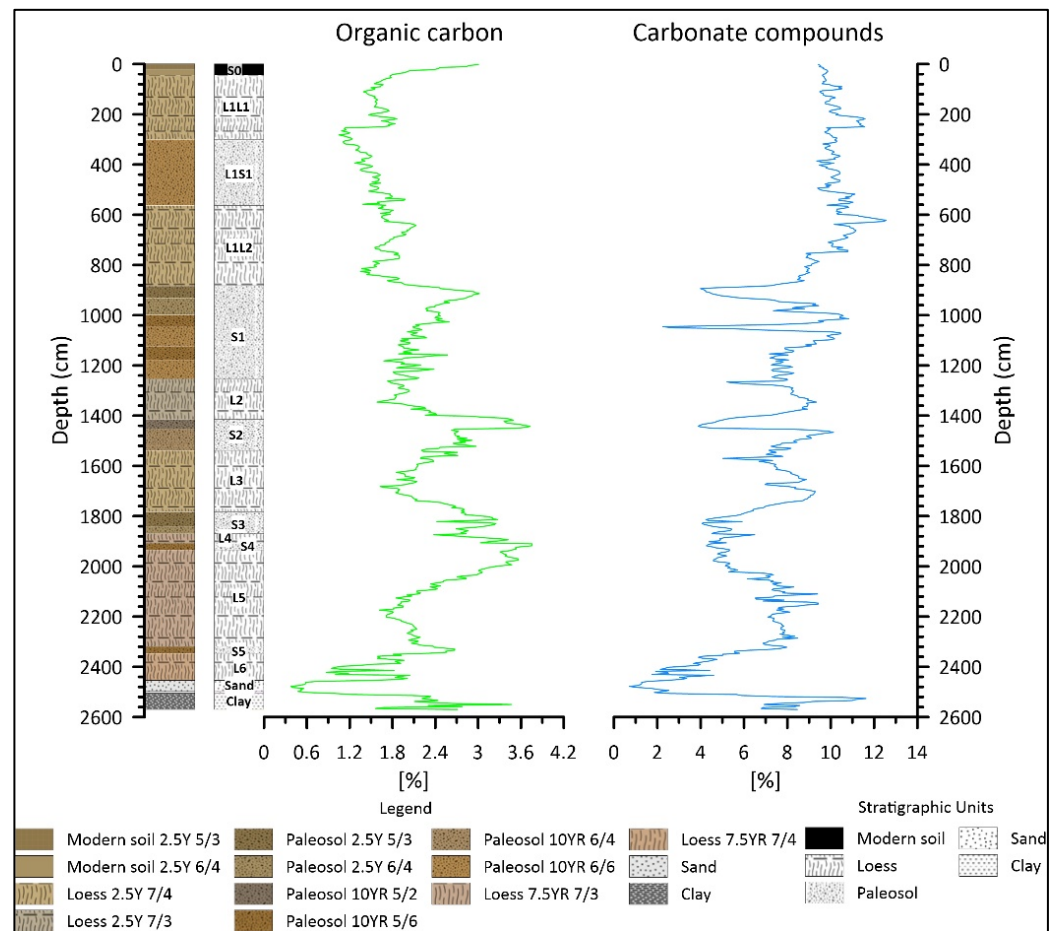


Figure 2. LOI results (Organic carbon: 550 °C, carbonate: 900 °C) of the Pécel section.

A thicker loess layer (L5) lies in the range 19.36–23.20 m, in which, the organic matter content decreases to 1.71% up to 21.92 m, while the carbonate content varies in the range 7.2–8.5%. Despite this variability, these values can still be considered stable compared to the layers below. Subsequently, organic matter content starts a significant increase from 21.92 m and reaches 3.5%. At the same time, carbonate content decreases with smaller and larger fluctuations, reaching 3.7%.

A thinner paleosol layer (S4) can be found again in the range 19.08–19.36 m. Within this paleosol, the proportion of organic matter content increases and the carbonate content decreases slightly upwards.

The uppermost loess (L4) layer examined within this study is located in the range 18.72–19.08 m. Herein, the organic matter content continuously increases from 3% to 3.4% and then decreases to 2.4% up to the paleosol horizon above it. In contrast, the carbonate content decreases from 5.2 to 4.4% and then increases to 6.5% by the boundary of the paleosol layer.

3.2.2. Kisdorog-West

The significant changes that were observed in the case of the Pécel profile cannot be detected here (Figure 3). The carbonate content constantly increases in the lower part of the lower loess layer (from 12% to 16% in the range 5.6–4 m). This value drops extremely at the depth of 4 m and reaches 2% up to 3.5 m. In contrast, it starts to increase up to the depth of 3 m by ~8% within the paleosol layer. Then, it starts to decrease again back to 4% between 3 and 2.5 m (the boundary of the paleosol and the upper loess layer), then increases to 10% up to the depth of 2 m. Subsequently, it decreases to 6% up to the depth of 1.6 m and then increases to 12% up to the horizon of the recent surface soil.

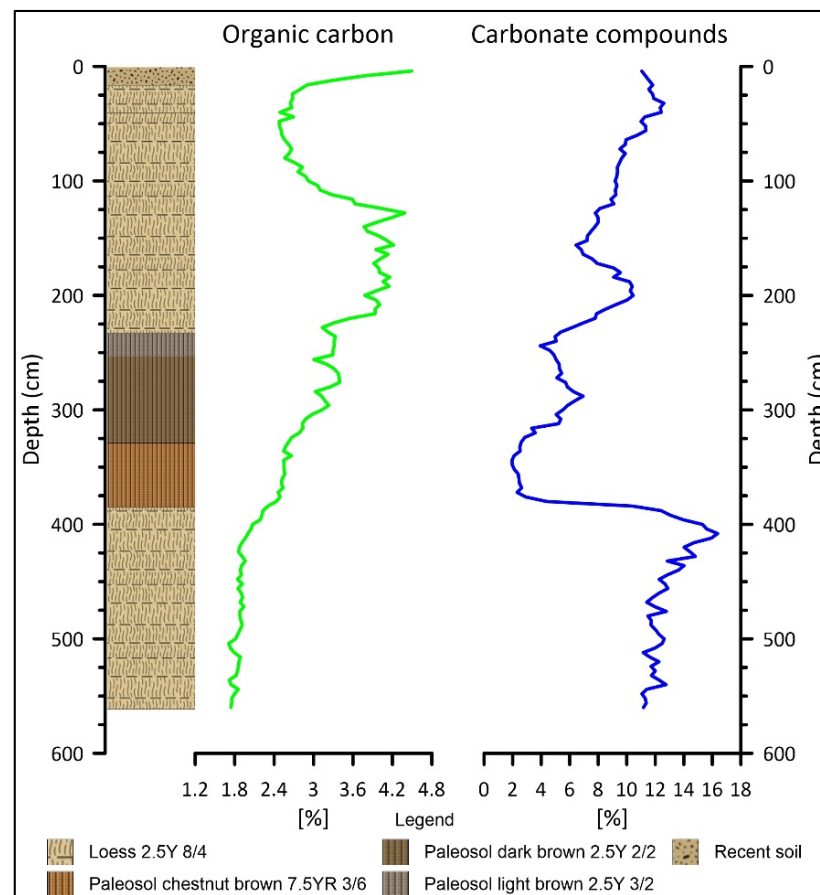


Figure 3. LOI results (organic carbon: 550 °C, carbonate: 900 °C) of the Kisdorog-West section.

The changes in organic matter content show even less variability. It increases continuously from ~1.8% to ~4.2% with smaller fluctuations between 5.6 and 1.5 m (the upper boundary of the loess). Above it, the value falls back to 2–2.4% and then reaches its maximum of ~4.4% in the recent surface soil level.

3.2.3. Kisdorog-East

This section, with its ~6.5-m height, contains a significant paleosol complex of nearly 3.5 m. However, as the Figure 4 shows, the organic matter content within this layer is still low (varying in the range 2–5%). The peak value of the organic matter can be observed within the recent soil layer with a value of almost 9%. At the same time, this value is constant ~2% on average within the loess bodies. The carbonate content is higher (around 8–10%) in the paleosol levels characterized by chestnut (7.5YR 3/6) and dark brown (2.5Y 2/2) color. A significant decrease to 4% is observed in the middle-positioned, light brown-colored (2.5Y 3/2) layer. In contrast to the paleosol layer, high carbonate contents (10–16%) were measured in both the lower and upper loess bodies.

3.2.4. Bonyhádvarasd

In the case of this profile, the organic matter content continuously increases in the lower loess body towards the paleosol complex (from 1.8% to 3%, Figure 5). A significant decrease (~2.2%) in the organic matter content can be observed in the lower, light brown layer of the paleosol, which is followed by an increase (to 3%) towards the chestnut-colored layer. Subsequently, it falls below 2% in the lower parts of the upper loess body, then starts to increase again upwards, and reaches its maximum of 4%.

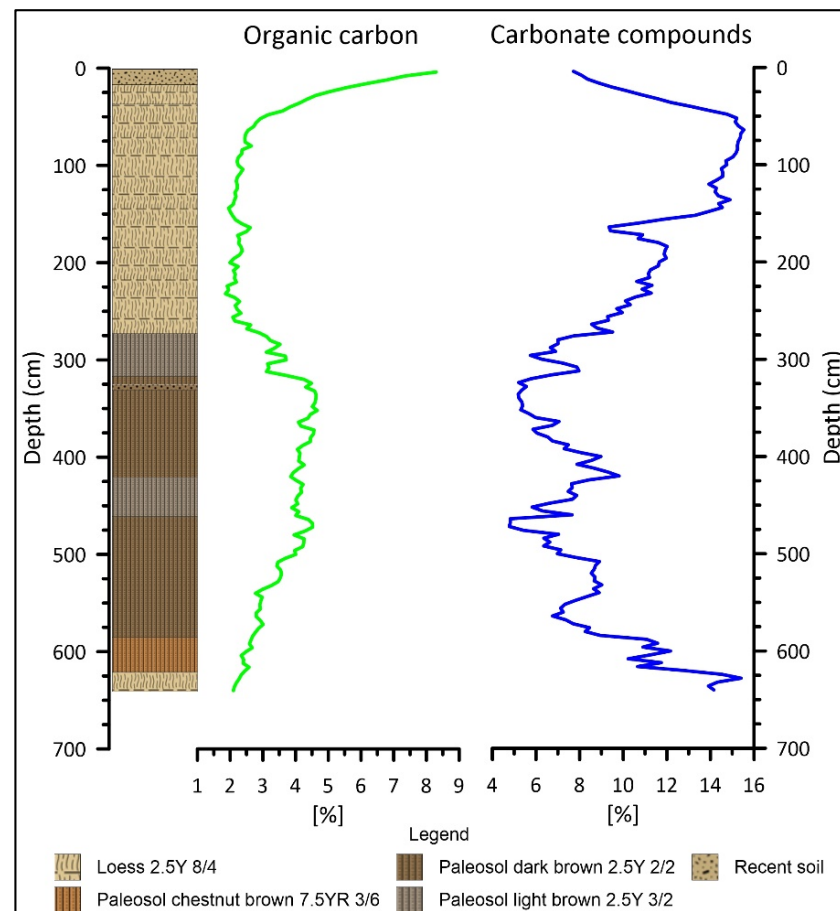


Figure 4. LOI results (organic carbon: 550 °C, carbonate: 900 °C) of the Kisdorog-East section.

The carbonate content increases upward from 13% to 18% within the lower loess body. At the depth of 6.08 m, where the loess–paleosol boundary is located, it drops drastically to ~2%. Its value reaches 8% in the paleosol complex; however, it falls back under 4% in the upper light brown (2.5Y 3/2) paleosol layer. Within the upper loess body, its value varies in the range 4–13%. The lowest carbonate content values are measured whereas the organic matter values are the highest. The recent soil cannot be detected clearly on the basis of these values only.

3.3. Grain Size Distribution

The profile of Pécel was the only examined one among the four where grain size fractions larger than very fine sand were detected. The main reason for this can be the sand deposits found below the loess body as well as the slight (more than 1%) fine sand content of the L1S1 paleosol horizon.

3.3.1. Pécel

It can be generally concluded that the proportion of very fine sand is significantly high (10%) in the entire section (Figure 6). Despite this fact, coarser sand fractions can be detected only in the fluvial sand layers at the bottom of the loess wall and do not reach 1% in the loess sediments above. In parallel with the general characteristics of loess walls [54], the two dominant grain size fractions are the medium (21.6%) and the coarse silt (30.6%).

Finer fractions become predominant in the range 25.07–25.72 m: 18.1% clay, 24.5% medium silt, and 26.4% coarse silt. In addition, an unusually high very fine sand ratio (8%) can be detected here as well.

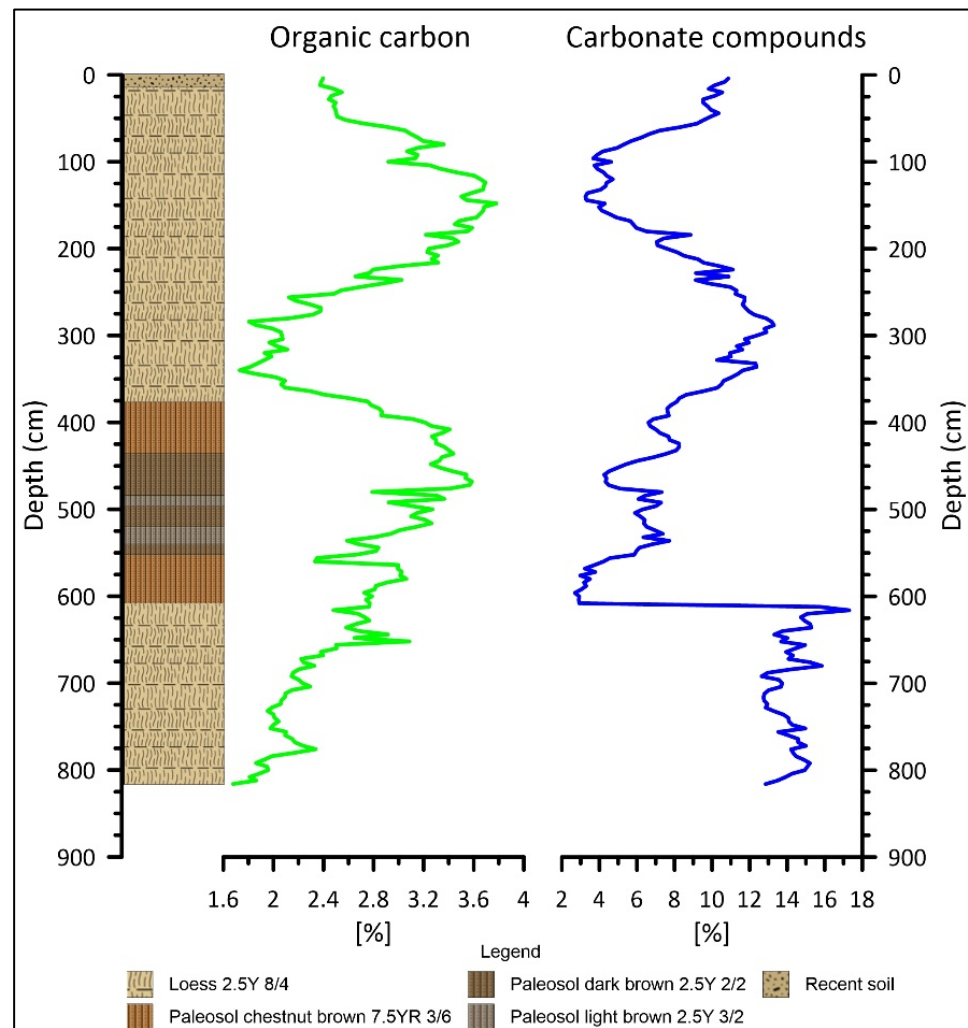


Figure 5. LOI results (organic carbon: 550 °C, carbonate: 900 °C) of the Bonyhádvarasd section.

The grain size composition of the sand body in the range 24.56–25.07 m is predominated by sand fractions. The proportion of the fine sand and larger fractions exceeds 1% only in this part within the entire section. However, the 15.5% proportion of very fine sand is combined with 35.8% fine sand and 10.3% medium sand here. An average ratio of 2.7% coarse sand can be detected as well.

Between 23.48 and 24.56 m, a loess body (L6) can be found. It can be characterized by a clay content of 17.5% and predominantly consists of medium (24.6%) and coarse (26.6%) silt. In addition, 8% of very fine sand can also be detected.

The S5 paleosol layer is located in the range 23.20–23.48 m. In this layer, a clay content of 19% can be detected, while the medium (24.6%) and coarse (27.4%) silt fractions are dominant here, with an additional 4.3% of very fine sand ratio.

Between 19.36 and 23.20 m, the proportion of medium silt (22.6%) decreases while the very fine sand (7.5%) increases compared to the paleosol below the L5 loess.

The paleosol layer (S4) in the range 19.08–19.36 m shows the highest clay content (19.9%) within the entire section. In addition, 23.6% of medium silt (close to the average) and 27.4% of coarse silt fractions can be detected as well. The proportion of very fine sand decreases to 5.8% here.

The L4 loess (in the range 18.72–19.08 m) is a thinner layer between 2 paleosol horizons, where the second highest clay (19.6%) content was measured. In this layer, the proportion of medium silt is similar to that in the paleosol below it. At the same time, the coarse silt increases to 29.7%, and the proportion of very fine sand decreases to 5%.

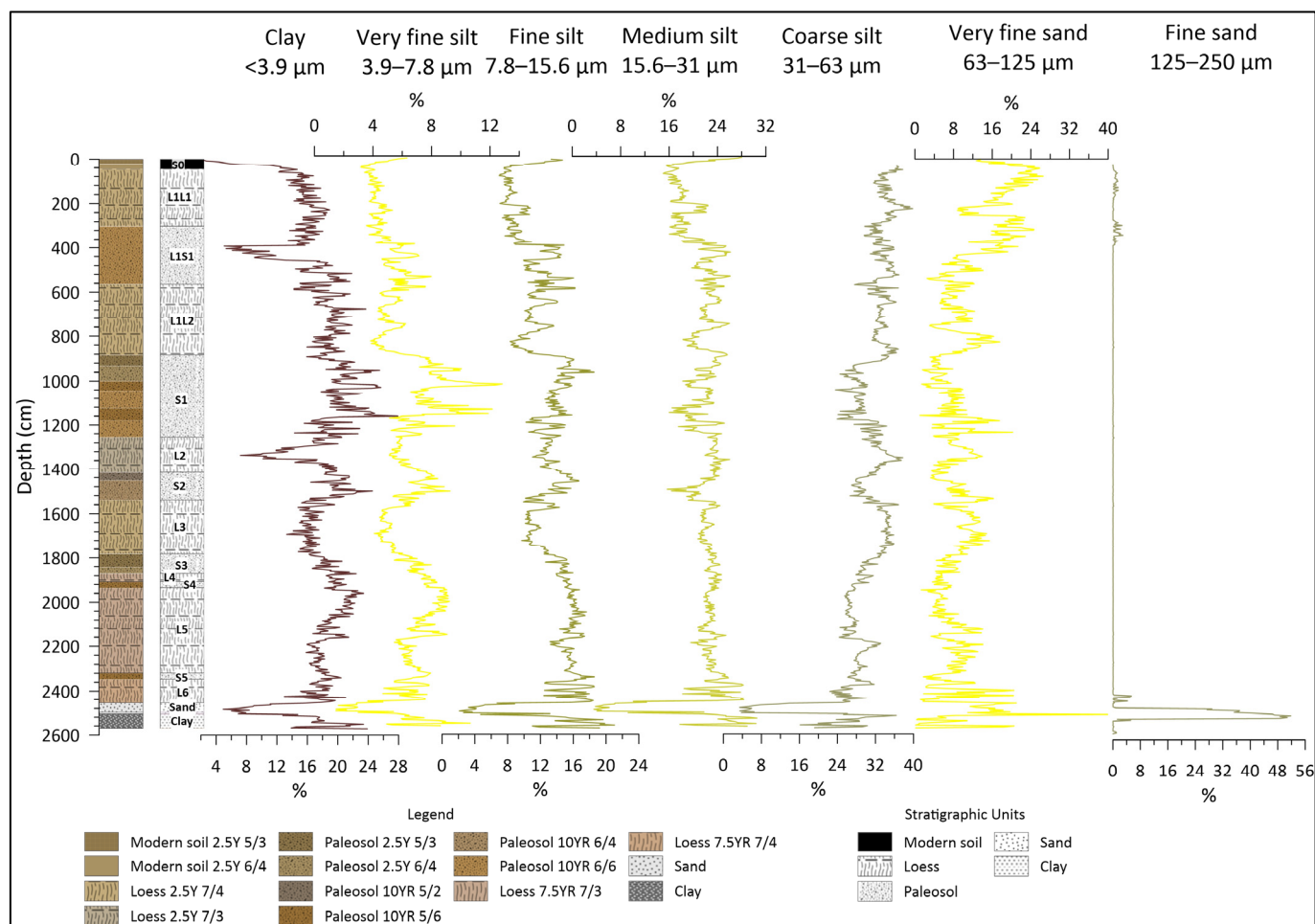


Figure 6. Grain size distribution of the Pécel section without medium and coarse sand.

3.3.2. Kisdorog-West

The dominant grain size fractions in the lower loess body (3.84–5.6 m) of this profile (Figure 7) are the coarse (35–39%) and medium (20–26%) silt. The proportion of the coarser fractions continuously decreases upwards against the finer fractions. At the same time, a relatively constant proportion of clay fraction was measured here (ranging between 16% and 24%). The proportion of the very fine sand fraction gradually decreases from its maximum of about 15% upwards to the paleosol complex (to 3.84 m), in which it almost completely disappears.

The grain size distribution of the paleosol complex (2.32–3.84 m) is dominated by finer fractions like clay and very fine silt that reach their maximum here (~28% and ~10%, respectively). At the boundary of the dark brown (2.5Y 2/2) and light brown (2.5Y 3/2) paleosol layers (2.52–2.76 m), the very fine silt fraction decreases from 10% to 6%.

Subsequently, the upper loess body (0.40–2.32 m) is dominated by medium and coarse silt; however, their proportions continuously decrease in parallel with the clay and very fine silt. A slight peak was detected in the proportion of very fine sand in the range 0.56–0.88 m, although it still does not exceed 1%.

The clay fraction decreases below 8% in the recent soil levels (0–0.4 m), which is the smallest value in the entire section. At the same time, this layer is also dominated by coarser fractions like coarse silt and even the proportion of the very fine sand increases and reaches 6%.

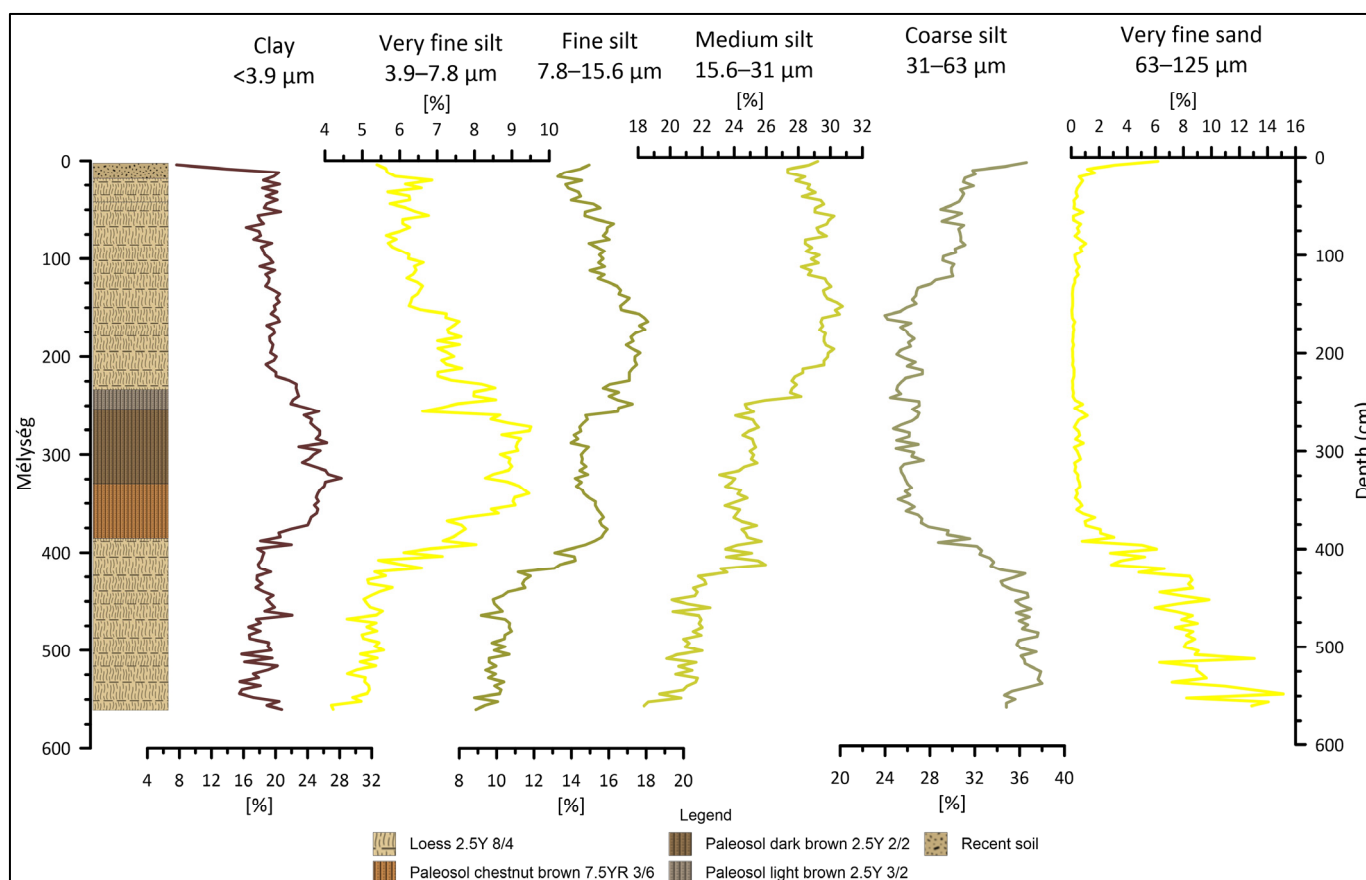


Figure 7. Grain size distribution of the Kisdorog-West section.

3.3.3. Kisdorog-East

Unlike the Western profile, the lower loess body (6.20–6.40 m) of the Eastern one (Figure 8) is dominated by medium silt (30–35%), as well as fine and coarse silt (22–28%). The proportion of the clay fraction decreases from 20% to 8% towards the boundary of the paleosol complex (6.20 m). Although the very fine sand fraction still can be detected here, its proportion is significantly less (maximum 4%).

The chestnut-brown-colored (7.5YR 3/6) layer (5.84–6.20 m) of the paleosol complex (in the range 2.72–6.20 m) is dominated by clay and medium silt (20–28%). Above it, the dark brown (2.5Y 2/2) layer (4.60–5.84 m) can be found, with a remarkable part between 5–5.50 m, where the proportion of the smaller fractions significantly increases against the coarse silt. At the boundary of the middle light brown (2.5Y 3/2, 4.10–4.60 m) and the upper dark brown (2.5Y 2/2, 2.16–4.20 m) paleosol layers, the proportion of the very fine and fine silt increases—similar to the lower dark brown (2.5Y 2/2) layer; however, the proportion of the medium and coarse silt decreases. At the same time, the proportion of the clay and very fine silt decreases at the lower boundary of the upper light brown (2.5Y 3/2) layer.

At the lower levels of the upper loess body (0.36–2.72 m), in the range 1.80–2.60 m, the proportion of the very fine sand increases to even 4% in some places. The proportion of the silt fractions continuously increases upwards the recent soil horizon, where they fall back in parallel with the increase of the very fine sand (up to ~8%).

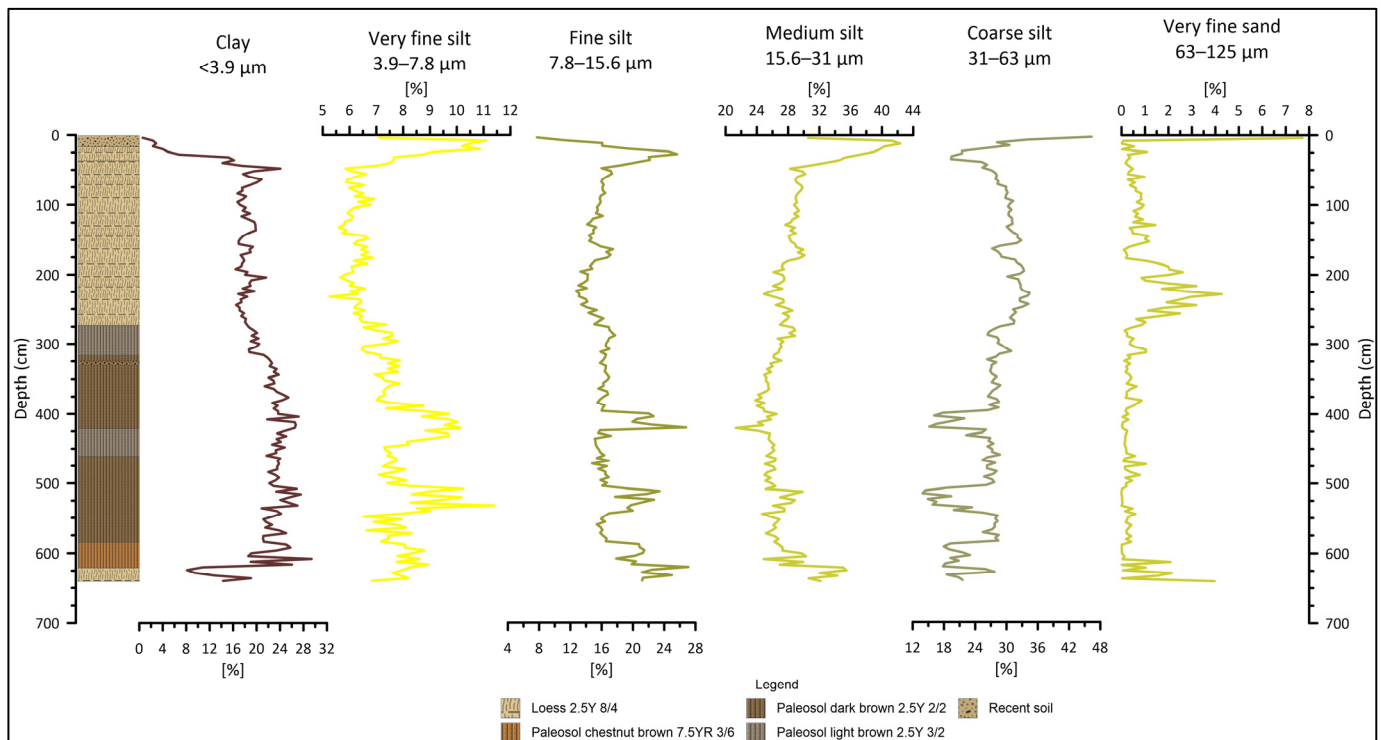


Figure 8. Grain size distribution of the Kisdorog-East section.

3.3.4. Bonyhádvarasd

The dominant grain size fraction of the lower loess body (6.08–8.16 m) of this profile (Figure 9) is medium silt with values varying in the range 22–33%. Concurrently, the proportion of clay fraction is also significant; the clay peak of the entire profile is detected here with a value of ~34%. In the upper part of the lower loess body, the proportion of fine silt increases by more than 10% against the coarse silt.

A contrary change can be detected at the boundary of the paleosol complex (3.76–6.08 m) and the lower loess body, where the coarse silt becomes dominant in addition to the medium silt. The shift of the middle light brown (2.5Y 3/2) and dark brown (2.5Y 2/2) layers (4.84–5.52) is hardly observable; however, the slight dominance of finer fractions can be detected. This trend reverses again in the upper dark brown (2.5Y 2/2) paleosol layer (4.36–4.84 m). These proportions fluctuate intensively within the upper chestnut-brown-colored (7.5YR 3/6) layer (3.76–4.36 m).

The following layer is the upper loess body (0.15–3.76 m). The lower parts of this level can be characterized by coarser fractions. In addition to the dominance of coarse silt, the clay fraction falls below an average of 10%, while an average of 8% of very fine sand can be detected with a maximum value of ~16%. The upper loess body is almost identical to the lower one in terms of grain composition.

3.4. Grain Size Indices

3.4.1. Pécel

The MGS value provides relatively less information in the case of the Pécel profile (Figure 10) due to the presence of the sandy sediment at the bottom of the section. The GSI and U-ratio values show a peak within the loess bodies and their trends are similar except for their trends in the L1S1 paleosol layer.

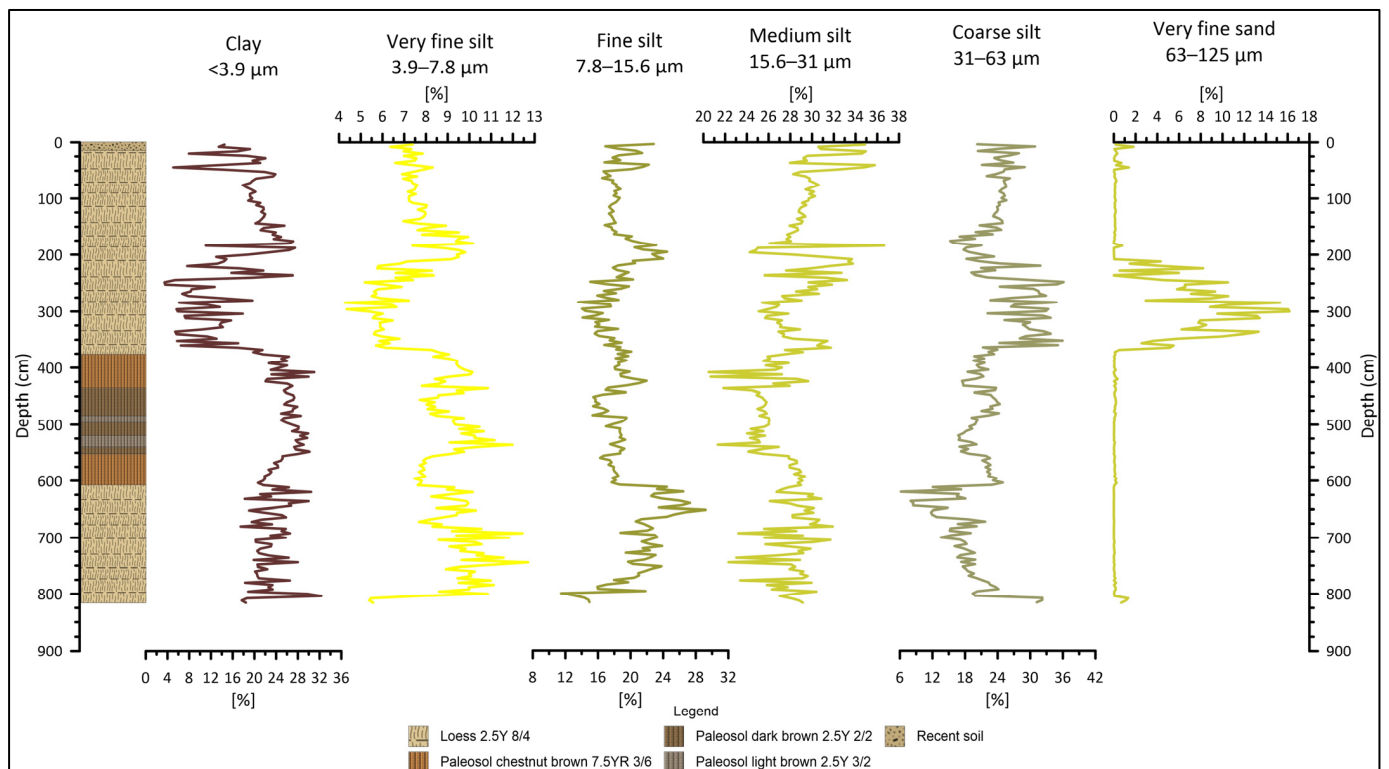


Figure 9. Grain size distribution of the Bonyhádvarasd section.

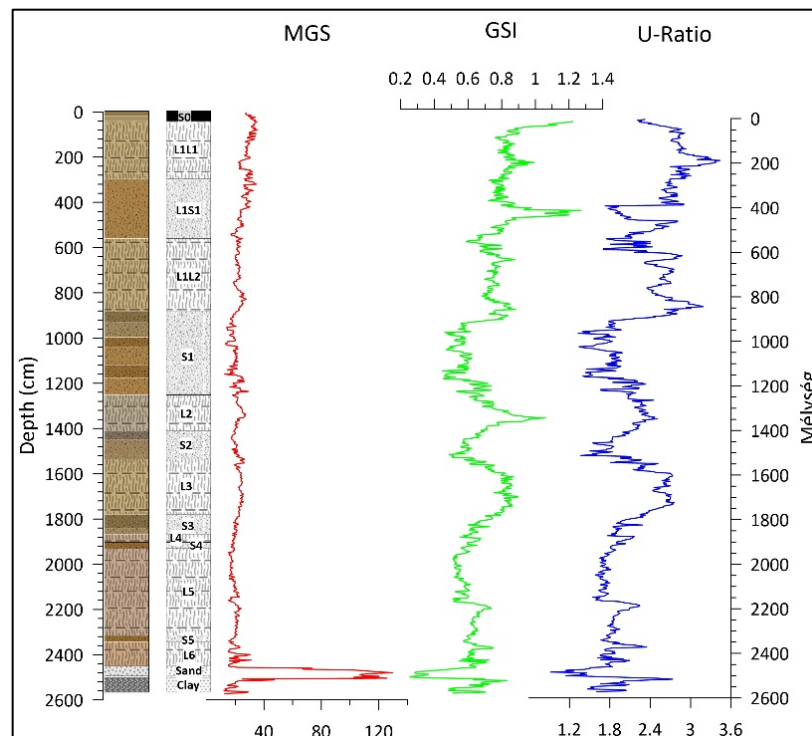


Figure 10. Mean grain size and grain size indices of the Pécel sequence.

3.4.2. Kisdorog-West

In Figure 11, we can see that all three indices show higher values within the lower loess body, while the lower values of the paleosol complex start to increase only from the middle of the upper loess body.

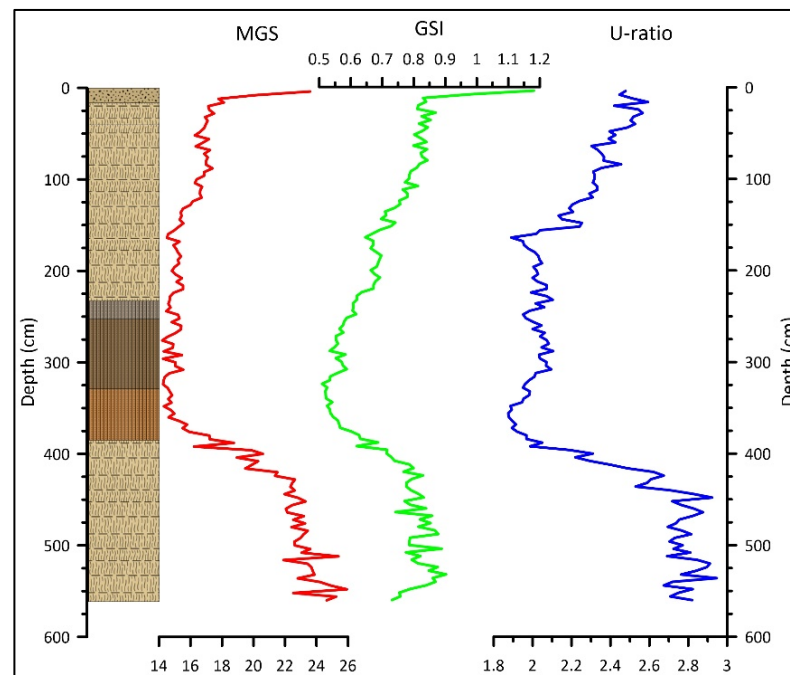


Figure 11. Mean grain size and grain size indices of the Kisdorog-West sequence.

3.4.3. Kisdorog-East

The GSI value is almost stable within the entire profile (Figure 12) except for some minor decreases. At the same time, the MGS and U-ratio values show two notable increases and a similarly significant decrease.

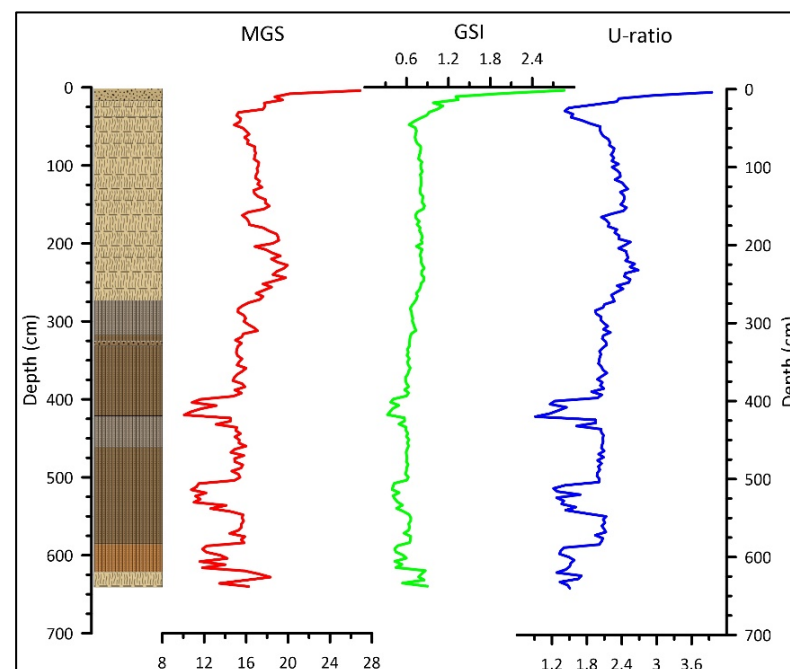


Figure 12. Mean grain size and grain size indices of the Kisdorog-East sequence.

3.4.4. Bonyhádvarasd

In the case of this profile (Figure 13), a significant increase can be observed for all three indices in the lower part of the upper loess body. Two parts with outstanding values of U-ratio can be seen in the paleosol complex.

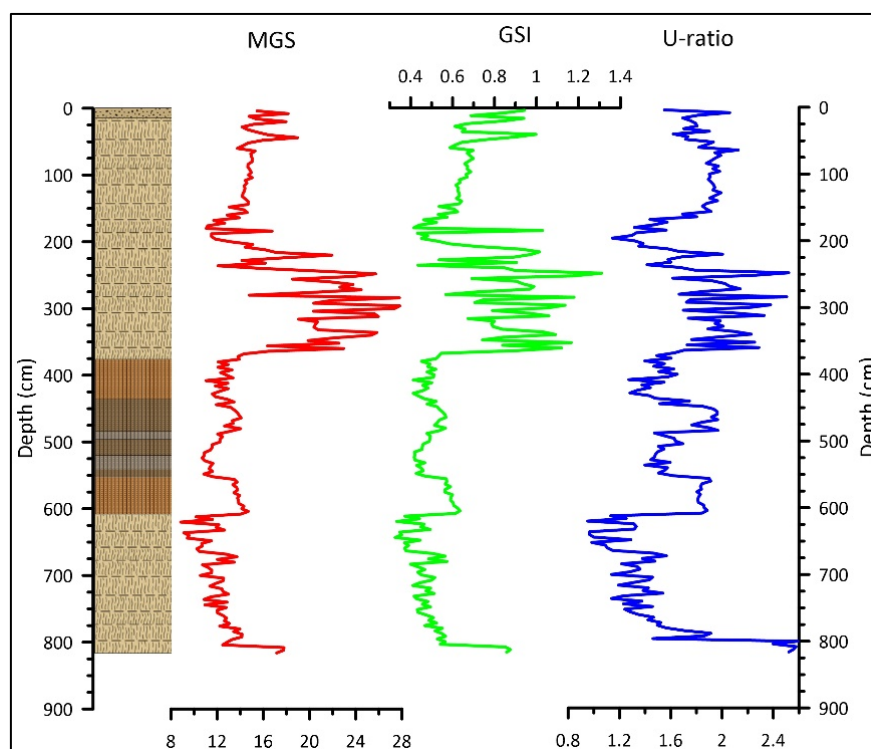


Figure 13. Mean grain size and grain size indices of the Bonyhádvarasd sequence.

3.5. Magnetic Susceptibility

Magnetic susceptibility values measured show high variability in the Pécel profile. The MS peak was detected in the upper part of the upper part of the L5 loess body with values of more than 100. For the rest of the profiles, only paleosol layers can be described with higher MS values. A double peak trend in the MS can be observed in the Transdanubian profiles; however, the upper peak can be observed in the upper loess body in the case of the Kisdorog-West section.

4. Discussion

4.1. Pécel

The periodical and permanent water cover characteristics of the fluvial areas suggest that intensive element mobilization may have occurred during the deposition of the fluvial sediments beneath the loess wall. The first stratum of these fluvial sediments is a clay layer. This is presumably a marsh sediment, the result of this former periodic water cover. A noticeable part of this section can be found in the range 25.20–25.40 m. At this depth, more than 10% carbonate content was measured.

The upper boundary of this red sand is a sand layer with a thickness of 51 cm. It contains massive, cross-layered, and laminated sand, in this order, from bottom to top. These sediments represent perfectly the development of the former stream's riverbed. Massive sand indicates a crevasse splay formation process, while cross-layered sand indicates turbulent, and laminated sand indicates laminar flow during the deposition of this sediment. The uppermost 7 cm of this sand layer is red-colored sand.

The L6 loess above, which was deposited on the fluvial sediment (with hiatus in some places), can be characterized by varying grain size composition and LOI values. In addition, fine sand can also be found in the lower parts of it. It can be assumed that the accumulation of the dust started in a period of temporary existing water coverage which may have mixed with the sand sediment underneath. The S5 layer above is a small paleosol horizon with a thickness of 28 cm.

Subsequently, a significant weathering horizon can be detected in the L5 loess body, predominated by finer grain size fractions. Subsequently, continuous soil development can be reconstructed based on the continuously increasing proportion of organic matter content towards the S4 paleosol layer. The outstanding GSI and U-ratio values in the range 21.80–21.92 m indicate an increase in wind velocity. Apart from this, no other significant change can be detected here.

The S4 paleosol layer is a small horizon of 28 cm, which cannot be detected clearly only on the basis of the changes in grain size distribution; however, it is clearly indicated by the shift of the Munsell colors and the LOI values. Above the S4 paleosol, a loess layer of 26 cm can be detected up to 18.72 m, where the paleosol of the previous section ended.

The subsequent L4 loess body is a small layer of only 36 cm; however, it could clearly be separated visually from the paleosols below and above it. The decrease in LOI values—a typical feature of loess sediments—can also be observed here.

The increase in both GSI and U-ratio values within the L3 loess body indicates an increase in wind and dust storm activities.

In the upper part of the S2 paleosol, the organic matter content increases significantly while the carbonate content values decrease, presumably due to leaching activity. Here, the grain size composition is dominated by finer fractions, and particle indices have declined significantly, indicating warming and a decrease in wind energy.

Above, clay fraction decreases significantly within the L2 loess body, while the proportion of the coarser fractions slightly increases in parallel with the increase of GSI values, indicating a significant increase in the transport energy.

In the S1 paleosol, horizons with significant decreases in carbonate content can be observed, which layers can be considered as leaching horizons. The grain size composition is dominated by finer fractions; thus, the particle indices are low, indicating low transport energy.

In the L1 complex, the L1L2 and L1L1 loess bodies are dominated by coarser fractions and higher particle indices, assuming a high wind activity during the accumulation of these layers. A significant decrease in clay proportion can be observed within the L1S1 paleosol. This is in parallel with the increase of the GSI values and the decrease of U-ratios. The formation of the paleosol layer indicates warming, which was interrupted by a cold period of stronger winds.

4.2. *Kisdorog-West*

This profile is divided into two loess bodies with a paleosol complex of three sublayers in between. The grain size composition results combined with the color analysis of the samples clearly indicate the paleosol layers. The lower loess body can be characterized by a high proportion of coarse silt and very fine sand. In addition, its carbonate content is low and MS values were measured in the range 10–20.

Among the three parameters gained from the LOI measurements, the low carbonate content is the one that clearly indicates the presence of the paleosol complex. Clay and very fine silt are the dominant grain size fractions here. High MS values can be detected in this section; however, the maximum value is only in the range 70–80.

The lower section of the upper loess body is dominated by fine and medium silt in addition to the extremely high organic matter content and high MS values as well. At the same time, the upper levels of this loess are dominated by coarser fractions with increased carbonate and decreased organic matter content.

The particle indices show increased values within the lower loess body while they decrease significantly up to the paleosol complex before start increase gradually up to the surface.

4.3. *Kisdorog-East*

This section is located 700 m away from the western one, on the eastern side of the loess hill. Its general structure is similar to the western one; 2 loess bodies with a paleosol

layer in between; however, this paleosol can be divided into five sublayers. The lower loess is of small size, where very fine sand can also be observed. It can be characterized by low organic matter and MS values.

Within the dark brown layers of this paleosol complex, 2 notable levels can be observed with high fine silt proportion compared to the coarser fractions. An increase in carbonate content can also be detected within these levels. MS values measured increase up to 150–160.

Very fine sand fraction occurs again in the lower levels of the upper loess body. From the depth of 150 cm upwards, carbonate content notably increases in addition to the shift of the grain size to the finer fractions.

Two notable levels of decrease in the grain size indices can be observed within the paleosol complex.

4.4. *Bonyhádvarasd*

Although this profile can be found 7 km away from the profiles of Kisdorog, it is quite similar to them in terms of structure. The paleosol complex of this profile can be divided into 7 sublayers with a 1–1 loess body above and below it similar to the ones of Kisdorog. The lower loess body can be characterized by constantly high carbonate as well as continuously increasing organ matter content upwards. The dominant grain size fraction is medium silt; however, the proportion of the clay fraction is also remarkable in this layer.

At the lower boundary of the paleosol complex, a significant decrease in the carbonate constant and a slight increase in the coarse silt fraction can be detected. The MS values are generally high in the paleosol layer and almost reach 160.

The very fine sand fraction appears in the lower levels of the upper loess body and its proportion reaches 16%. At this level, the organic matter decreases below 2% accompanied by 10–12% carbonate content. In its upper section, the particle size is shifted towards the finer fractions. In addition, the highest organic matter content in the entire section (3–4%) was also measured here.

Similar to the Kisdorog-East profile, a significant decrease and then increase of the particle indices can be observed within the paleosol complex, although the highest values here were measured in the lower parts of the upper loess body.

5. Conclusions

The relative ages of the profiles could be determined by the comparison of the MS values measured here to the values obtained from the study of the Chinese Loess Plateau (Figures 14 and 15). Due to its size, among other factors, more information can be extracted by the examination of the profile of Pécel than from the three other ones studied in this paper. By comparing the MS values with the one measured in the case of the Chinese Loess Plateau, this profile can be traced back to the MIS 9–10 stages. The deposition of the other three (Transdanubian) profiles can presumably be dated back to the MIS 2–4; moreover, they can be parallelized with the L1L1-L1S1-L1L2 strata of the Pécel profile.

5.1. *Pécel*

The development of the loess wall and the deposition of its sediments began with the southward movement of the stream. The variable sand content indicates a periodically increasing wind energy and velocity of which traces can be detected in the different layers deposited. However, only smaller periods of time can be characterized by this high wind velocity.

Ostracods were found in the clay sediment at the bottom of the section, suggesting an Upper Miocene age of the sediment. Based on the presence of this Upper Miocene stratum, the erosion of the lowermost part of the profile can be assumed and the deposition of the loess sediment began after the termination of the fluvial sediment.

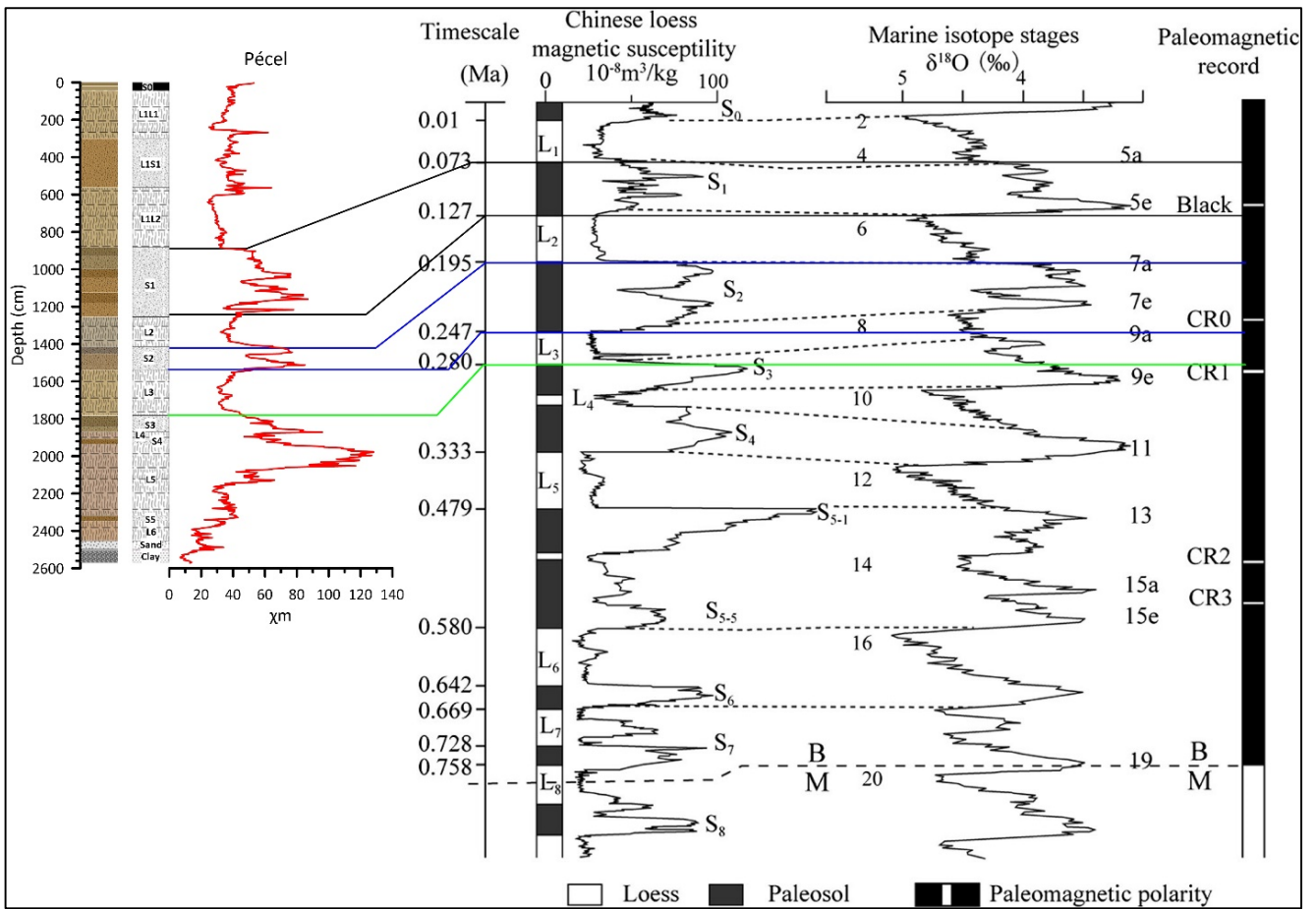


Figure 14. MS comparisons between the Pécel sections and the Chinese Loess Plateau [55]. The black lines describe the S1 paleosol, the blue ones the S2, and the green line is the beginning of the S3 paleosol of the Chinese loess sequence.

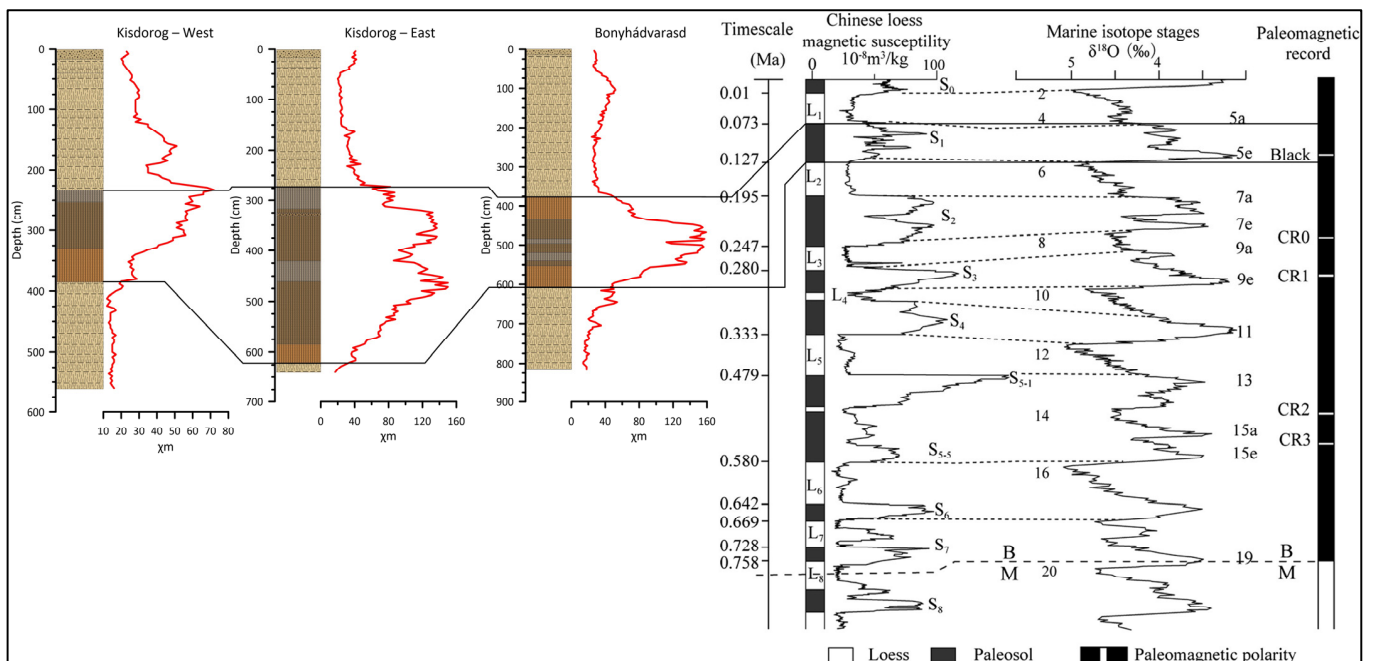


Figure 15. MS comparisons between the Transdanubian sections and the Chinese Loess Plateau [55].

5.2. Transdanubian Profiles

In the case of the three Transdanubian profiles, significant differences can be observed compared to the Pécel one. The topography of the hill area in the surroundings of the examined profiles can be characterized by northwest–southeast-oriented hills. Based on the grain size analysis, very fine sand fraction can be detected in the lower loess body of Kisdorog-West and Kisdorog-East and in the upper loess body of the Bonyhádvarasd profiles. This suggests that the prevailing wind direction was north–northwest during the deposition of the lower layers and south–southeast during the deposition of the upper layers. The significant changes observed in the particle indices also support this assumption for the paleosol complexes. In addition, it can be concluded that the eastern-oriented profile includes less-developed paleosol horizons. In its case, only three sublayers could be distinguished and the MS values barely reached 80, while they increased to 150–160 in the cases of the other two profiles.

Author Contributions: Conceptualization, L.M., D.M., and P.S.; methodology, L.M. and D.M.; software, L.M. and D.M.; validation, L.M. and D.M.; formal analysis, P.C.; investigation, L.M., D.M., P.C., and B.N.; resources, L.M. and P.S.; data curation, L.M.; writing—original draft preparation, L.M.; writing—review and editing, L.M., D.M., and P.C.; visualization, L.M. and D.M.; supervision, P.S.; project administration, L.M. and D.M.; funding acquisition, L.M. All authors have read and agreed to the published version of the manuscript.

Funding: This research was funded by the Hungarian Government, Ministry of Human Capacities (20391-3/2018/FEKUSTRAT), the Hungarian National Excellence Program grant NTP-NFTÖ-21-B-0063 (L. Makó), and the European Regional Development Fund, grant number: GINOP-2.3.2-15-2016-00009 ‘ICER’.

Data Availability Statement: The data presented in this study are available on request from the corresponding author.

Acknowledgments: Initial expressions of gratitude are to Gedeon Rajcsinec for his stewardship of the Pécel area and to Illés Vinery of the Kisdorog area, which facilitated the preservation of the loess walls and enabled our investigation. Additionally, our appreciation extends to all individuals who participated in this research endeavor.

Conflicts of Interest: The authors declare no conflict of interest.

References

1. Dövényi, Z. *Cserhát-Vidék in Magyarország Kistájainak Katasztere*, 2nd ed.; MTA Földrajztudományi Kutatóintézet: Budapest, Hungary, 2010; pp. 705–708.
2. Sümegi, P.; Gulyás, S.; Persaits, G.; GergelyPáll, D.; Molnár, D. The loess-paleosol sequence of Basaharc (Hungary) revisited: Mollusc-based paleoecological results for the Middle and Upper Pleistocene. *Quat. Int.* **2011**, *240*, 181–192. [[CrossRef](#)]
3. Böskén, J.; Obreht, I.; Zeeden, C.; Klasen, N.; Hambach, U.; Sümegi, P.; Lehmkuhl, F. High-resolution paleoclimatic proxy data from the MIS3/2 transition recorded in northeastern Hungarian loess. *Quat. Int.* **2019**, *502*, 95–107. [[CrossRef](#)]
4. Sümegi, P.; Törőcsik, T.; Náfrádi, K.; Sümegi, B.P.; Majkut, P.; Molnár, D.; Tapody, R. Radiocarbon dated complex paleoecological and geoarcheological analyses at the Bodrogkeresztúr Henye Gravettian site (NE Hungary). *Archeom. Műhely* **2016**, *8*, 31–42.
5. Makó, L.; Molnár, D.; Cseh, P.; Sümegi, P. MAR comparisons between different chronometric methods for two profiles in the Bodrogkeresztúr area. *Stud. Quat.* **2021**, *38*, 67–73.
6. Varga, A.; Újvári, G.; Raucsik, B. Tectonic versus climatic control on the evolution of a loess-paleosol sequence at Beremend, Haungary: An integrated approach based on paleoecological, clay mineralogical, and geochemical data. *Quat. Int.* **2011**, *240*, 71–86. [[CrossRef](#)]
7. Dövényi, Z. *Mecsek és Tolna-Baranyai-Dombvidék in Magyarország Kistájainak Katasztere*, 2nd ed.; MTA Földrajztudományi Kutatóintézet: Budapest, Hungary, 2010; pp. 500–503.
8. Sümegi, P.; Náfrádi, K.; Molnár, D.; Sávai, S. Results of paleoecological studies in the loess region of Szeged-Öthalom (SE Hungary). *Quat. Int.* **2015**, *372*, 66–78. [[CrossRef](#)]
9. Sümegi, P.; Molnár, D.; Gulyás, S.; Náfrádi, K.; Sümegi, B.P.; Törőcsik, T.; Persaits, G.; Molnár, M.; Vandenberghe, J.; Zhou, L. High-resolution proxy record of the environmental response to climatic variations during transition MIS3/MIS2 and MIS2 in Central Europe: The loess-paleosol sequence of Katymár brickyard (Hungary). *Quat. Int.* **2019**, *504*, 40–55. [[CrossRef](#)]

10. Sümegi, P.; Gulyás, S.; Molnár, D.; Szilágyi, G.; Sümegi, B.P.; Törőcsik, T.; Molnár, M. 14C Dated Chronology of the Thickest and Best Resolved Loess/Paleosol Record of the LGM from SE Hungary Based on Comparing Precision and Accuracy of Age-Depth Models. *Radiocarbon* **2020**, *62*, 403–417. [[CrossRef](#)]
11. Molnár, D.; Sümegi, P.; Makó, L.; Cseh, P.; Zeeden, C.; Nett, J.; Lehmkuhl, F.; Törőcsik, T.; Sümegi, B.P. Palaeoecological background of the Upper Palaeolithic site of Ságvár, Hungary: Radiocarbon-dated malacological and sedimentological studies on the Late Pleistocene environment. *J. Quat. Sci.* **2021**, *36*, 1353–1363. [[CrossRef](#)]
12. Sümegi, P.; Gulyás, S.; Molnár, D.; Bozsó, G.; Fekete, I.; Makó, L.; Cseh, P.; Molnár, M.; Sümegi, B.P.; Almond, P.; et al. New chronology and extended palaeoenvironmental data to the 1975 loess profile of Madaras brickyard, South Hungary. *J. Quat. Sci.* **2021**, *36*, 1364–1381. [[CrossRef](#)]
13. Molnár, D.; Makó, L.; Sümegi, P.; Sümegi, B.P.; Törőcsik, T. Revisiting the palaeolithic site at Szeged-Öthalom: Attempt for appoint the palaeolithic horizon. *Stud. Quat.* **2019**, *36*, 45–53.
14. Újvári, G.; Varga, A.; Raucsik, B.; Kovács, J. The Paks loess-paleosol sequence: A record of chemical weathering and provenance for the last 800ka in the mid-Carpathian Basin. *Quat. Int.* **2014**, *319*, 22–37. [[CrossRef](#)]
15. Újvári, G.; Molnár, M.; Páll-Gergely, B. Charcoal and mollusc shell 14 C-dating of the Dunaszekcső loess record, Hungary. *Quat. Geochronol.* **2016**, *35*, 43–53. [[CrossRef](#)]
16. Buggle, B.; Glaser, B.; Zöller, L.; Hambach, U.; Marković, S.B.; Glaser, I.; Gerasimenko, N. Geochemical characterization and origin of Southeastern and Eastern European loesses (Serbia, Romania, Ukraine). *Quat. Sci. Rev.* **2008**, *27*, 1058–1075. [[CrossRef](#)]
17. Marković, S.B.; Bokhorst, M.P.; Vandenberghe, J.; McCoy, W.D.; Oches, E.A.; Hambach, U.; Gaudenyi, T.; Jovanović, M.; Zöller, L.; Stevens, T.; et al. Late Pleistocene loess-palaeosol sequences in the Vojvodina region, north Serbia. *J. Quat. Sci.* **2008**, *23*, 73–84. [[CrossRef](#)]
18. Marković, S.B.; Stevens, T.; Kukla, G.J.; Hambach, U.; Fitzsimmons, K.E.; Gibbard, P.; Buggle, B.; Zech, M.; Guo, Z.; Hao, Q.; et al. Danube loess stratigraphy—Towards a pan-European loess stratigraphic model. *Earth-Sci. Rev.* **2015**, *148*, 228–258. [[CrossRef](#)]
19. Galović, L.; Frechen, M.; Halamić, J.; Durn, G.; Romić, M. Loess chronostratigraphy in Eastern Croatia—A luminescence dating approach. *Quat. Int.* **2009**, *198*, 85–97. [[CrossRef](#)]
20. Molnár, D.; Hupuczi, J.; Galović, L.; Sümegi, P. Preliminary malacological investigation on the loess profile at Zmajevac, Croatia. *Open Geosci.* **2010**, *2*, 52–56. [[CrossRef](#)]
21. Molnár, D.; Makó, L.; Cseh, P.; Sümegi, P.; Fekete, I.; Galović, L. Middle and Late Pleistocene loess-palaeosol archives in East Croatia: Multi-proxy palaeoecological studies on Zmajevac and Šarengrad II sequences. *Stud. Quat.* **2021**, *38*, 3–17.
22. Makó, L.; Molnár, D.; Runa, B.; Bozsó, G.; Cseh, P.; Nagy, B.; Sümegi, P. Selected Grain-Size and Geochemical Analyses of the Loess-Paleosol Sequence of Pécel (Northern Hungary): An Attempt to Determine Sediment Accumulation Conditions and the Source Area Location. *Quaternary* **2021**, *4*, 17. [[CrossRef](#)]
23. Koloszár, L.; Marsi, I. The thickest and the most complete loess sequence in the Carpathian Basin: The section of the borehole Udvari-2A and its significance in the Quaternary stratigraphy (in Hungarian). *Földtani Közlemény* **2010**, *140*, 251–262.
24. Sümegi, P.; Gulyás, S.; Molnár, D.; Sümegi, B.P.; Almond, P.C.; Vandenberghe, J.; Zhou, L.; Pál-Molnár, E.; Törőcsik, T.; Hao, Q.; et al. New chronology of the best developed loess/paleosol sequence of Hungary capturing the past 1.1 ma: Implications for correlation and proposed pan-Eurasian stratigraphic schemes. *Quat. Sci. Rev.* **2018**, *191*, 144–166. [[CrossRef](#)]
25. Wikimedia Commons. Pannonian Basin Geographic Map Blank Cropped. Available online: https://upload.wikimedia.org/wikipedia/commons/2/27/Pannonian_Basin_geographic_map_blank_cropped.svg (accessed on 15 May 2021).
26. Sümegi, P.; Hertelendi, E. Reconstruction of microenvironmental changes in Kopasz Hill loess area at Tokaj (Hungary) between 15,000–70,000 BP years. *Radiocarbon* **1998**, *40*, 855–863. [[CrossRef](#)]
27. Munsell Color (Firm). *Munsell Soil Color Charts: With Genuine Munsell Color Chips*; Munsell Color: Grand Rapids, MI, USA, 2010.
28. Nettleton, W.D.; Brasher, B.R.; Benham, E.C.; Ahrens, R.J. A classification system for buried paleosols. *Quat. Int.* **1998**, *51–52*, 175–183. [[CrossRef](#)]
29. Kraus, M.J. Paleosols in clastic sedimentary rocks: Their geologic applications. *Earth-Sci. Rev.* **1999**, *47*, 41–70. [[CrossRef](#)]
30. Krasilnikov, P.; García Calderón, N.E. A WRB-based buried paleosol classification. *Quat. Int.* **2006**, *156–157*, 176–188. [[CrossRef](#)]
31. Dean, W.E. Determination of carbonate and organic matter in calcareous sediments and sedimentary rocks by loss on ignition; comparison with other methods. *J. Sediment. Res.* **1974**, *44*, 242–248. [[CrossRef](#)]
32. Heiri, O.; Lotter, A.F.; Lemcke, G. Loss on ignition as a method for estimating organic and carbonate content in sediments: Reproducibility and comparability of results. *J. Paleolimnol.* **2001**, *25*, 101–110. [[CrossRef](#)]
33. Bokhorst, M.P.; Vandenberghe, J.; Sümegi, P.; Łanczont, M.; Gerasimenko, N.P.; Matviishina, Z.N.; Marković, S.B.; Frechen, M. Atmospheric circulation patterns in central and eastern Europe during Weichselian Pleniglacial inferred from loess grain-size records. *Quat. Int.* **2011**, *234*, 62–74. [[CrossRef](#)]
34. Wentworth, C.K. A scale of grade and class terms for clastic sediments. *J. Geol.* **1922**, *30*, 377–392. [[CrossRef](#)]
35. Vandenberghe, J.; Mucher, H.J.; Roebroeks, W.; Gemke, D. Lithostratigraphy and Palaeoenvironment of the Pleistocene Deposits at Maastricht-Belvédère, Southern Limburg, the Netherlands in Maastricht-Belvédère: Stratigraphy, Palaeoenvironment and Archaeology of the Middle and Late Pleistocene Deposits. *Analecta Praehist. Leiden.* **1985**, *18*, 7–18.
36. Vandenberghe, J.; An, Z.S.; Nugteren, G.; Lu, H.; van Huissteden, K. New absolute time scale for Quaternary climate in the Chinese Loess region by grain-size analysis. *Geology* **1997**, *25*, 35–38. [[CrossRef](#)]
37. Vandenberghe, J.; Nugteren, G. Rapid climatic changes recorded in loess successions. *Glob. Planet. Chang.* **2001**, *28*, 1–9. [[CrossRef](#)]

38. Nugteren, G.; Vandenberghe, J.; van Huissteden, K.; An, Z.S. A Quaternary climate record based on grain size analysis from the Luochuan loess section on the Central Loess Plateau, China. *Glob. Planet. Chang.* **2004**, *41*, 167–183. [[CrossRef](#)]
39. Vandenberghe, J. Grain size of fine-grained windblown sediment: A powerful proxy for process identification. *Earth-Sci. Rev.* **2013**, *121*, 18–30. [[CrossRef](#)]
40. Rousseau, D.; Antoine, P.; Hatté, C.; Lang, A.; Zöller, L.; Fontugne, M.; Othman, D.; Luck, J.; Moine, O.; Labonne, M.; et al. Abrupt millennial climatic changes from Nussloch (Germany) Upper Weichselian eolian records during the Last Glaciation. *Quat. Sci. Rev.* **2002**, *21*, 1577–1582. [[CrossRef](#)]
41. Rousseau, D.-D.; Sima, A.; Antoine, P.; Hatté, C.; Lang, A.; Zöller, L. Link between European and North Atlantic abrupt climate changes over the last glaciation. *Geophys. Res. Lett.* **2007**, *34*, 22713. [[CrossRef](#)]
42. Újvári, G.; Kok, J.F.; Varga, G.; Kovács, J. The physics of wind-blown loess: Implications for grain size proxy interpretations in Quaternary paleoclimate studies. *Earth-Sci. Rev.* **2016**, *154*, 247–278. [[CrossRef](#)]
43. Zhou, L.P.; Oldfield, F.; Wintle, A.G.; Robinson, S.G.; Wang, J.T. Partly pedogenic origin of magnetic variations in Chinese loess. *Nature* **1990**, *346*, 737–739. [[CrossRef](#)]
44. An, Z.; Kukla, G.J.; Porter, S.C.; Xiao, J. Magnetic Susceptibility Evidence of Monsoon Variation on the Loess Plateau of Central China during the last 130,000 Years. *Quat. Res.* **1991**, *36*, 29–36. [[CrossRef](#)]
45. Rousseau, D.D.; Kukla, G. Late Pleistocene Climate Record in the Eustis Loess Section, Nebraska, Based on Land Snail Assemblages and Magnetic Susceptibility. *Quat. Res.* **1994**, *42*, 176–187. [[CrossRef](#)]
46. Dearing, J.A.; Hay, K.L.; Baban, S.M.J.; Huddleston, A.S.; Wellington, E.M.H.; Loveland, P.J. Magnetic susceptibility of soil: An evaluation of conflicting theories using a national data set. *Geophys. J. Int.* **1996**, *127*, 728–734. [[CrossRef](#)]
47. Sun, J.; Liu, T. Multiple origins and interpretations of the magnetic susceptibility signal in Chinese wind-blown sediments. *Earth Planet. Sci. Lett.* **2000**, *180*, 287–296. [[CrossRef](#)]
48. Zhu, R.; Liu, Q.; Jackson, M.J. Paleoenvironmental significance of the magnetic fabrics in Chinese loess-paleosols since the last interglacial (<130 ka). *Earth Planet. Sci. Lett.* **2004**, *221*, 55–69.
49. Hlavatskyi, D.; Bakhmutov, V. Early-Middle Pleistocene Magnetostratigraphic and Rock Magnetic Records of the Dolynske Section (Lower Danube, Ukraine) and Their Applications to the Correlation of Loess-Palaeosol Sequences in Eastern and South-Eastern Europe. *Quaternary* **2021**, *4*, 43. [[CrossRef](#)]
50. Chen, J.; Chen, Y.; Liu, L.; Ji, J.; Balsam, W.; Sun, Y.; Lu, H. Zr/Rb ratio in the Chinese loess sequence and its implication for changes in the East Asian winter monsoon strength. *Geochim. Cosmochim. Acta* **2006**, *70*, 1471–1482. [[CrossRef](#)]
51. Kukla, G. Loess stratigraphy in central China. *Quat. Sci. Rev.* **1987**, *6*, 191–219. [[CrossRef](#)]
52. Kukla, G.; An, Z. Loess stratigraphy in Central China. *Palaeogeogr. Palaeoclimatol. Palaeoecol.* **1989**, *72*, 203–225. [[CrossRef](#)]
53. Kukla, G.; An, Z.S.; Melice, J.L.; Gavin, J.; Xiao, J.L. Magnetic susceptibility record of Chinese Loess. *Trans. R. Soc. Edinb. Earth Sci.* **1990**, *81*, 263–288. [[CrossRef](#)]
54. Pye, K. The nature, origin and accumulation of loess. *Quat. Sci. Rev.* **1995**, *14*, 653–667. [[CrossRef](#)]
55. Ren, J.; Zhang, S.; Meigs, A.J.; Yeats, R.S.; Ding, R.; Shen, X. Tectonic controls for transverse drainage and timing of the Xin-Ding paleolake breach in the upper reach of the Hutuo River, north China. *Geomorphology* **2014**, *206*, 452–467. [[CrossRef](#)]

Disclaimer/Publisher’s Note: The statements, opinions and data contained in all publications are solely those of the individual author(s) and contributor(s) and not of MDPI and/or the editor(s). MDPI and/or the editor(s) disclaim responsibility for any injury to people or property resulting from any ideas, methods, instructions or products referred to in the content.